Journal of Nuclear Medicine, published on November 30, 2017 as doi:10.2967/jnumed.117.201293

PSMA-11 Derived Dual-labeled PSMA-Inhibitors for Preoperative PET Imaging and Precise Fluorescence-Guided Surgery of Prostate Cancer

Ann-Christin Baranski[1,*], Martin Schäfer[1], Ulrike Bauder-Wüst[1], Mareike Roscher[1], Jana Schmidt[1], Esther Stenau[2], Tobias Simpfendörfer[3], Dogu Teber[3], Lena Maier-Hein[2], Boris Hadaschik[4], Uwe Haberkorn[5,6], Matthias Eder[7,†], Klaus Kopka[1,8,†]

[1] Div. of Radiopharmaceutical Chemistry, German Cancer Research Center (DKFZ), Heidelberg, Germany
[2] Div. of Computer-Assisted Medical Interventions (CAMI), German Cancer Research Center (DKFZ), Heidelberg, Germany
[3] Department of Urology, Heidelberg University Hospital, Heidelberg, Germany
[4] Department of Urology, University Hospital Essen, Essen, Germany
[5] Department of Nuclear Medicine, Heidelberg University Hospital, Heidelberg, Germany
[6] Clinical Cooperation Unit Nuclear Medicine, German Cancer Research Center (DKFZ), Heidelberg, Germany
[7] Div. of Radiopharmaceutical Development, German Cancer Consortium (DKTK), Department of Nuclear Medicine, University Medical Center, Freiburg, Germany
[8] German Cancer Consortium (DKTK), Heidelberg, Germany

[†] These authors contributed equally to this work and share last authorship.

* First and Corresponding author:
Ann-Christin Baranski
Doctoral student
Radiopharmaceutical Chemistry, German Cancer Research Center (DKFZ)
Im Neuenheimer Feld 280
69120 Heidelberg
Tel: +49 6221 422431
Fax: +49 6221 422434
Mail: a.baranski@dkfz.de

Word count of the manuscript: 4994

Financial support: BMBF/VIP+ (VP00130)

Short running title: Dual-Labeled PSMA-11

ABSTRACT

Resection of tumor lesions using targeted dual-modality probes combining preoperative imaging with intraoperative guidance is of high clinical relevance and might considerably impact the outcome of prostate cancer therapy. This work aims at the development of dual-labeled prostate specific membrane antigen (PSMA)-inhibitors derived from the established positron emission tomography (PET)- and N,N'-bis[2-hydroxy-5-(carboxyethyl)benzyl]ethylenediamine-N,N'-diacetic acid (HBED-CC) based tracer ^{68}Ga-Glu-urea-Lys(Ahx)-HBED-CC (^{68}Ga-PSMA-11) to allow accurate intraoperative detection of PSMA-positive tumor lesions. **Methods:** A series of novel PSMA-targeting fluorescent dye conjugates of Glu-urea-Lys-HBED-CC were synthesized and their biological properties determined in cell based assays and confocal microscopy. As a preclinical proof-of-concept, specific tumor uptake, pharmacokinetics and feasibility for intraoperative fluorescence-guidance were investigated in tumor-bearing mice and healthy pigs. **Results:** The designed dual-labeled PSMA-inhibitors exhibit high binding affinity and PSMA-specific effective internalization. Conjugation of Fluoresceinisothiocyanate (FITC) (10.86±0.94 %ID/g), IRDye800CW (13.66±3.73 %ID/g) and DyLight800 (15.62±5.52 %ID/g) resulted in a significantly increased specific tumor uptake, while ^{68}Ga-Glu-urea-Lys-HBED-CC-AlexaFluor488 (9.12±5.47 %ID/g) revealed a similar tumor uptake as compared to ^{68}Ga-PSMA-11 (4.89±1.34 %ID/g). First proof-of-concept studies with the clinically relevant candidate ^{68}Ga-Glu-urea-Lys-HBED-CC-IRDye800CW reinforce a fast specific enrichment in PSMA-positive tumors with rapid background clearance. With regard to intraoperative navigation a specific fluorescence signal was detected in PSMA-expressing tissue. **Conclusion:** This study demonstrates that PSMA-11 derived dual-labeled dye-conjugates are feasible to provide

PSMA-specific pre-, intra- and postoperative detection of prostate cancer lesions and have high potential for future clinical translation.

Key words: fluorescence-guided surgery, PET imaging, prostate cancer, PSMA-11

INTRODUCTION

Precise detection and resection of tumor tissue is of major importance for the treatment outcome and survival of patients. In prostate cancer, tumor visualization by multiparametric magnetic resonance imaging or hybrid imaging has improved significantly over the past years*(1)*. Despite the excellent preoperative localization of tumor lesions with diagnostic radiopharmaceuticals, the entirely surgical resection of tumor tissue remains challenging*(2,3)*. Hence, surgical intervention of prostate cancer comprises the risk of tumor tissue left behind thereby increasing the potential of cancer recurrence*(4)*. As a result, there is still a huge demand to improve the intraoperative navigation of the surgeon by further simplifying the discrimination between malignant and healthy tissue.

Besides radio-guided navigation, intraoperative near infrared imaging shows promising advances to improve the care of prostate cancer patients*(5,6)*. The non-targeting agents methylene blue and indocyanine green (ICG) represent the first FDA (Food and Drug Administration) approved compounds with near infrared fluorescence properties for clinical use. However, combining radionuclide and near infrared imaging in dual-modality agents has been proved to merge the strength of both techniques*(7)*. The application of dual-modality ICG-^{99m}Tc-NanoColloids was one of the first approaches emphasizing the improved surgical accuracy by detecting sentinel lymph nodes with combined radioactive and fluorescent signal in first clinical proof-of-concept-studies*(8)*.

However, non-targeted imaging has its limitations to visualize residual tumor lesions. Due to tumor-independent enrichment of non-targeted probes a precise discrimination between tumor and healthy tissue cannot be provided. In the case of

dual-modality ICG-^{99m}Tc-NanoColloids a distribution along the lymphatic system enables the detection of sentinel lymph nodes in the lymphatic drainage area of the primary tumor. Due to the regional application, a high enrichment close to the injection side causes enhanced background in the pelvic area and lesions outside the lymphatic distribution route might not be identified*(7)*.

To overcome these restrictions dual-labeled probes targeting specifically prostate cancer cells have been developed. The prostate specific membrane antigen (PSMA) has been identified to be overexpressed in prostate cancer*(9)*. As the upregulation of PSMA correlates with the malignancy of the carcinoma*(10)*, PSMA became an established target for the diagnosis and therapy of prostate cancer. Besides mono-modality probes providing either radionuclide*(11-16)* or fluorescence imaging*(17-20)*, only a few antibody or small molecule based dual-modality agents targeting the extracellular domain of PSMA have been designed previously*(21,22)*. While for antibody approaches specific tumor visualization is hampered due to long circulation in the blood pool, small molecule probes show faster pharmacokinetics resulting in clear imaging contrast at early time points post injection. Since biological properties of small molecules are typically affected by their conjugation with chelators or fluorescent dyes, the challenge in the design of dual-modality probes is to preserve favorable pharmacokinetic properties along with a high and specific tumor uptake.

In this study, the clinically established PET-tracer ^{68}Ga-Glu-urea-Lys(Ahx)-HBED-CC (^{68}Ga-PSMA-11) was selected as a low molecular weight PSMA-inhibitor core structure, showing fast clearance from blood and background organs with a high specific uptake in prostate cancer lesions*(12,23,24)*. Here, we present the preclinical evaluation

of novel dual-labeled PSMA-inhibitors based on PSMA-11 with advantageous pharmacokinetics and considerably improved targeting properties for sensitive pre-, intra-, and postoperative detection of prostate cancer.

MATERIALS AND METHODS

Chemical Synthesis and Radiolabeling

All commercially available chemicals, reagents and solvents were of analytical grade and used without further purification. The synthesis of the bis-tetrafluorophenyl-functionalized HBED-CC was performed as described previously*(25)*. The product with the tetrafluorophenyl activated sites (0.157 mmol) was reacted with tri-tert-butyl protected Glu-urea-Lys (purchased from ABX, Radeberg, Germany; 0.9 eq., 0.141 mmol, 68.90 mg) in dimethylformamide in the presence of 25 µl *N*,*N*-diisopropylethylamine. After 4 h at RT an excess of 100 µl 2,2′-(ethylenedioxy)bis(ethylamine) was added and the mixture was reacted for 16 h at RT to form tri-*tert*-butyl protected Glu-urea-Lys[Fe(HBED-CC)]-PEG_2-NH_2. The activated dyes FITC (Isomer I, Merck, Darmstadt, Germany; 1 eq., 1 mg) and AlexaFluor488-tetrafluorophenyl ester (Thermo Fisher Scientific, Waltham, USA; 1 eq., 1 mg), respectively, were solved in 50 µl dimethyl sulfoxide and conjugated to Glu-urea-Lys[Fe(HBED-CC)]-PEG_2-NH_2 (3 eq.) in dimethylformamide (300µl) and *N*,*N*-diisopropylethylamine (15 µl) for 24 h at RT. The conjugation of IRDye800CW-NHS-ester (LI-COR Biosciences, Bad Homburg, Germany; 1 eq., 1 mg) and Dylight800-NHS-ester (Thermo Fisher Scientific, Waltham, USA; 1 eq., 1 mg), respectively, to Glu-urea-Lys[Fe(HBED-CC)]-PEG_2-NH_2 was performed in phosphate buffered saline (PBS, pH 8.5, 300 µl) for 24 h at RT. Complexed Fe^{3+} was removed on a Sep-Pack C18 cartridge (Waters, Eschborn, Germany) with 1 M HCl as described previously*(25)*. The final conjugates were purified and analyzed by reversed-phased high-performance liquid chromatography (RP-HPLC) and matrix-assisted laser desorption/ionization mass

spectrometry (MALDI-MS) (Table 1). To further characterize the precursor Glu-urea-Lys[Fe(HBED-CC)]-PEG_2-NH_2 additionally high-resolution MS and NMR were performed (the supplemental materials provide detailed method information).

^{68}Ga (half-life 68 min; β^+ 89%; $E_{\beta+}$ max. 1.9 MeV) was obtained from a pyrogallol resin support based ^{68}Ge/^{68}Ga generator*(26)*. For ^{68}Ga-labeling the precursor peptides [1 nmol in 2-[4-(2-hydroxyethyl)piperazin-1-yl]ethanesulfonic acid buffer (580 mg/ml) with 5 mg ascorbic acid, 90 µL] were added to 40 µL [^{68}Ga]Ga^{3+} eluate (~40 MBq). The pH was adjusted to 3.8 using NaOH, typically 1-2 µl of 30% NaOH were sufficient. The reaction mixture was incubated at 98°C for 10 minutes. The radiochemical yield (RCY) was determined by analytic RP-HPLC and reversed phase thin- layer chromatography (RP-TLC) on silica gel plates (60 RP-18F_{254S}; Merck, Darmstadt, Germany) with 0.1 M sodium citrate as a mobile phase. For $^{69/71}$Ga-complexation the precursor peptides (1 mM in 0.1 M 2-[4-(2-hydroxyethyl)piperazin-1-yl]ethanesulfonic acid buffer, pH 7.5, 40 µl, 40 nmol) were reacted with a 10 fold molar excess of Ga(III)-nitrate (Sigma-Aldrich, in 0.1 N HCl, 10 µl) in a mixture of 10 µl of 2-[4-(2-hydroxyethyl)piperazin-1-yl]ethanesulfonic acid solution (2.1 M) over night at room temperature. The pH of the labeling solution was adjusted to 4.2 using NaOH. The lipophilicity of the ^{68}Ga-labeled compounds was determined using the 2-phase system n-octanol and PBS.

Cell Culture

PSMA-positive LNCaP cells (ATCC CRL-1740) and PSMA-negative PC3 cells (ATCC CRL-1435) were cultured in RPMI medium enriched with 10% fetal calf serum and 2 mmol/L L-glutamine (all from PAA, Etobicoke, Canada). Cells were grown at 37°C

in humidified air with 5% CO_2 and were harvested using trypsin-ethylenediaminetetraacetic acid (trypsin-EDTA; 0.25% trypsin, 0.02% EDTA, Invitrogen).

Cell Binding and Internalization

The competitive cell binding assay and internalization experiments were performed as described previously*(12)*. Briefly, competitive binding was done by incubating various concentrations of $^{69/71}$Ga labeled or non-complexed compound in the presence of ^{68}Ga-labeled radioligand [Glu-urea-Lys(Ahx)]$_2$-HBED-CC (PSMA-10, ABX, Radeberg, Germany). Internalization was determined by incubation of 30 nM radiolabeled compound for 45 min at 37 °C and at 4 °C, respectively. 500 µM of 2-(phosphonomethyl)-pentanedioic acid (2-PMPA) were used for blocking studies. Cell-bound radioactivity and the collected fractions were measured using a gamma counter (Packard Cobra II, GMI, Minnesota, USA).

Microscopy

For confocal microscopy, 10^5 cells were seeded in poly-L-lysine coated 4 well Nunc™ Lab-Tek™ II Chamber Slides™ (Thermo Fisher Scientific, Waltham, USA) 48 h before incubation. After washing once with PBS, cells were incubated with 300 µl non-complexed Glu-urea-Lys-HBED-CC-AlexaFluor488 (10 nM) in medium supplemented with 10% fetal calf serum and 2 mmol/L L-glutamine (all from PAA, Etobicoke, Canada) for 5, 15 or 30 min, respectively. Blocking studies were performed by incubating 10 nM solution of non-complexed Glu-urea-Lys-HBED-CC-AlexaFluor488 for 30 min in the presence of 2-PMPA (500 µM). After incubation, cells were washed with PBS and fixed for 10 min with paraformaldehyde (2% in PBS). After washing three times with PBS the chamber was removed. For mounting one drop of ProLong™ Diamond Antifade

Mountant with DAPI (Thermo Fisher Scientific, Waltham, USA) per well was used and the slides covered with 0.17 ± 0.1 mm (Karl Hecht, Sondheim, Germany) cover glass. The cellular uptake and internalization of the non-complexed Glu-urea-Lys-HBED-CC-AlexaFluor488 was measured using the confocal microscope Leica TCS SP5 II (Leica, Wetzlar, Germany) equipped with an 63x/ 1.40 OIL objective (lens). The measurement was performed with 405 nm diode and Argon laser (488 nm) with a detection window of 415 to 484 nm (DAPI) and 498 to 587 nm (Glu-urea-Lys-HBED-CC-AlexaFluor488).

Biodistribution and Imaging Studies

For the experimental mouse tumor models 5×10^6 cells of LNCaP or PC3 (in 50% Matrigel; Becton Dickinson, Heidelberg, Germany), respectively, were subcutaneously inoculated into the right trunk of 7- to 8-week-old male BALB/c nu/nu mice (Charles River Laboratories, Wilmington, USA). The tumors were allowed to grow until approximately 1 cm^3 in size. For organ distribution studies, the ^{68}Ga-labeled compounds were injected into a tail vein (1-2 MBq; 60 pmol, n=3). The animals were sacrificed at 1, 2 or 6 h post injection. Organs of interest were dissected, blotted dry, and weighed. The radioactivity was measured using a gamma counter and calculated as % ID/g.

For small-animal PET studies, mice were anaesthetized (2 % sevoflurane, Abbott, Wiesbaden, Germany) and placed into a PET scanner (Inveon PET, Siemens, Erlangen, Germany). After a 10 min transmission scan, 0.5 nmol of the ^{68}Ga-labeled compounds in 0.9% NaCl (pH=7) were injected in the tail vein and a 60 min dynamic scan and a static scan from 120 to 140 min were obtained (n=1). The reconstruction of the images was iteratively (16 subsets, 4 iterations) applying median root prior correction and converted to standardized uptake value (SUV) images. For the small-animal proof of concept

study, LNCaP tumor-bearing mice underwent µPET imaging for 2 h after injection of 0.5 nmol ^{68}Ga-Glu-urea-Lys-HBED-CC-IRDye800CW. Afterwards tumor and PSMA-expressing tissue was detected and resected by fluorescence-guidance using an IMAGE1 S system by KARL STORZ GmbH & Co. KG (Tuttlingen, Germany, excitation wavelength 805 nm). In a further proof of concept study, healthy pigs (2-3 month old, n=2) were anesthetized and after pre-injection imaging acquisition with da Vinci FireFly system by Intuitive Surgical, Inc. (Sunnyvale, California, USA, excitation wavelength 805 nm), 1 mg non-complexed Glu-urea-Lys-HBED-CC-IRDye800CW (30 µg/kg in sterile PBS) was intravenously administered. One hour post injection the fluorescence signal was detected and fluorescence-guided prostatectomy including *ex vivo* fluorescence-control performed. All animal experiments complied with the current laws of the Federal Republic of Germany and were conducted according to German Animal Welfare guidelines.

Statistical Aspects

Experiments were performed at least in triplicate. Quantitative data were expressed as mean ± SD. If applicable, means were compared using Student´s *t* test (GraphPad Prism Version 7). *P* values < 0.05 were considered statistically significant.

RESULTS

In Vitro Characterization

The final products could be identified using RP-HPLC/MALDI-MS and Glu-urea-Lys[Fe(HBED-CC)]-PEG_2-NH_2 as the PSMA-11 derived precursor was proven to be fully consistent to the assigned structure by high resolution MS and NMR (Supplemental Figs. 1-10). In order to investigate the influence of the fluorescent dye-conjugation to the PSMA-11 derived precursor, internalization efficiency and PSMA-binding affinity were determined (Table 2). The ^{68}Ga complexation of all investigated compounds resulted in radiochemical yields > 99%. Lipophilicity of the ^{68}Ga-labeled compounds was investigated by logD determination in comparison to ^{68}Ga-PSMA-11(-2.91 ± 0.06) and ranged from -2.01 to -2.98 (Supplemental Table 1).

All dye-conjugates showed a high complexation-independent PSMA-binding affinity in the same nanomolar range as compared to the reference PSMA-11*(25,27)*. In contrast to the slightly reduced specific cell surface binding, the specific internalization was improved for the ^{68}Ga- and dye-labeled compounds with a strong significant enhancement for ^{68}Ga-Glu-urea-Lys-HBED-CC-IRDye800CW by a factor of 3.9 ($p<0.05$).

Specific cell binding and internalization could also be visualized by confocal microscopy (Fig. 1). The evaluated compound Glu-urea-Lys-HBED-CC-AlexaFluor488 (non-complexed) showed an increased binding and intracellular fraction for PSMA-positive LNCaP cells over time, while for PSMA-negative PC3 cells almost no uptake was detected. Simultaneous incubation with 2-PMPA, a highly specific PSMA-inhibitor, resulted in successful blocking of Glu-urea-Lys-HBED-CC-AlexaFluor488 uptake.

In Vivo Characterization

Besides high PSMA-binding affinity and excellent internalization properties, dye conjugation to the PSMA-11 derived core structure resulted in a high tumor uptake in PSMA-expressing tumors (Fig. 2A, Supplemental Table 3). As compared to the reference ^{68}Ga-PSMA-11 (4.89±1.34 %ID/g)*(27)*, tumor uptake was significantly increased for the ^{68}Ga-labeled conjugates with FITC (10.86±0.94 %ID/g, factor: 2.2, $p<0.05$), IRDye800CW (13.66±3.73 %ID/g, factor: 2.8, $p<0.05$), and DyLight800 (15.62±5.52 %ID/g, factor: 3.2, $p<0.05$), while ^{68}Ga-Glu-urea-Lys-HBED-CC-AlexaFluor488 showed a similar tumor uptake (9.12±5.47 %ID/g, factor: 1.9, $p>0.05$). The tumor uptake was proved to be specific, as a strongly reduced uptake in PSMA-negative PC3 tumors was obtained for all conjugates (Supplemental Table 4). Besides a higher tumor uptake after dye- conjugation, pharmacokinetic properties of PSMA-11 were preserved meaning excellent background clearance and renal excretion of all conjugates. A typical uptake in PSMA-expressing spleen tissue was also observed (Fig. 2A, Supplemental Table 3)*(10)*.

Due to their near infrared fluorescence, ^{68}Ga-Glu-urea-Lys-HBED-CC-IRDye800CW and ^{68}Ga-Glu-urea-Lys-HBED-CC-DyLight800 are well suited for further clinical translation. In comparison, both conjugates have a similar tumor uptake ($p>0.05$), but tumor-to-organ ratios for relevant background organs appear to be higher for the IRDye800CW-conjugate (^{68}Ga-Glu-urea-Lys-HBED-CC-IRDye800CW: Tumor/Blood=4.49, Tumor/Heart=4.92, Tumor/Lung=2.44, Tumor/Liver=4.94, Tumor/Muscle=4.78; ^{68}Ga-Glu-urea-Lys-HBED-CC-DyLight800: Tumor/Blood=2.18,

Tumor/Heart=3.43, Tumor/Lung=1.90, Tumor/Liver=2.54, Tumor/Muscle=4.06) (Supplemental Table 5).

An additional organ distribution study over different time points was performed with the candidate for clinical translation, ^{68}Ga-Glu-urea-Lys-HBED-CC-IRDye800CW (Fig. 2B, Supplemental Table 6). After a significant reduction two hours post injection (7.94±0.19 %ID/g, $p<0.05$), the tumor uptake was only slightly decreased between two and six hours post injection (6.57±0.63 %ID/g, $p<0.05$), suggesting a stabilization of tumor uptake at later time points. Particularly, tumor/background organ ratios were strongly increased over time, indicating that the unspecific uptake was reduced to a minimum after six hours (six hours post injection: Tumor/Blood=15.56, Tumor/Heart=12.87, Tumor/Lung=6.88, Tumor/Liver=6.43, Tumor/Muscle=12.85) (Supplemental Table 7).

Small-animal PET studies confirmed the findings from the organ distribution study showing clear visualization of the PSMA-positive tumor with fast clearance from background organs for all conjugates comparable to ^{68}Ga-PSMA-11 *(12)* (Fig. 3, Supplemental Fig. 11). In PSMA-negative PC3 tumors ^{68}Ga-labeled dye-conjugate enrichment in tumor tissue was not observed, proving high PSMA-specificity of the examined conjugates.

Proof-of-Concept Studies

Beside the successful visualization of PSMA-positive tumors in small-animal PET, a PSMA-specific fluorescence signal in the tumor tissue could be detected *ex vivo* (Fig. 4 A, Supplemental Fig. 12), while background organs (e.g. muscle) appeared grey in the fluorescence mode using ^{68}Ga-Glu-urea-Lys-HBED-CC-IRDye800CW. A fluorescence

signal in kidney and spleen was also measured as these organs have a physiological PSMA-expression*(10)*. As an additional setting closer to clinical surgery studies in healthy pigs were performed with the da Vinci robotic system after injection of non-complexed Glu-urea-Lys-HBED-CC-IRDye800CW (Fig. 4 B). One hour post injection a PSMA-specific fluorescence signal was observed in the prostate expressing PSMA on a physiological level, while surrounding background tissue appeared in grey in the surgeon's console. After prostatectomy under fluorescence-guidance, fluorescence was confirmed *ex vivo*, showing a signal in prostate tissue and no signal for surrounding soft tissue (Supplemental Fig. 13).

DISCUSSION

In the therapy of prostate cancer, precise resection of primary and/or metastatic tumor lesions has a strong influence on patient outcome. New approaches comprising dual-labeled probes hereby support the surgeon for more simplified preoperative planning by means of PET/computed tomography or PET/magnetic resonance imaging combined with precise intraoperative navigation assistance. This dual-modality technology unites localization of tumor foci through the radioactive signal prior surgery with intraoperative radio-guidance and highly accurate fluorescence-guided comprehensive resection of tumor tissue.

The feasibility to implement such treatment regimen in a clinical work flow was previously demonstrated by van der Poel et al.*(8)* with multimodal ICG-^{99m}Tc-NanoColloids visualizing sentinel lymph nodes. This rather unspecific approach can be overcome by targeted probe design*(21,22)*. Due to their favorable pharmacokinetic properties, in particular fast clearance from the blood pool accompanied by high tumor-to-background contrast at early time points, low molecular weight PSMA-inhibitors provide an optimal basis for the design of dual-modality probes. PSMA-11 was identified to be the ideal core molecule with successful implementation in the clinical working routine as a PET-tracer for the imaging of prostate cancer*(1,23,24)*. The high clinical impact of PSMA-11 on treatment regimen is emphasized by recent studies, reporting a change in patient management after ^{68}Ga-PSMA-11 PET in approximately 50% of men*(28)*. Further developed by additional conjugation of a fluorescent dye, dual-labeled PSMA-ligands derived from PSMA-11 might considerably improve prostate cancer therapy precisely guiding the surgeon to tumor lesions. The ^{68}Ga-labeled fluorescent-

dye conjugates presented in this study exhibit high PSMA-binding affinity with strongly increased internalization efficiency. These excellent targeting characteristics resulted in up to factor 3.2 improved specific tumor uptakes in PSMA-positive lesions with high tumor-to-background contrasts as early as one hour post injection as compared to ^{68}Ga-PSMA-11. This might be attributed to the introduction of aromatic groups through fluorescent dyes, potentially resulting in a further enhancement of the interaction within the PSMA-binding pocket as lipophilic and aromatic motives have previously been reported to be advantageous*(29)*. The dyes represent lipophilic structures, preferably located distal to the glutamic acid moiety for improved inhibitory potency*(30)*. As features like polarity, size, charge and flexibility also have to be taken into account, the diverse coupled dyes consequently perform slightly different in terms of their influence on binding properties. No correlation between overall lipophilicity and tumor uptake has been observed. The higher tumor uptake might be also attributed to the longer circulation in the blood, which typically also increases the tumor accumulation of biomolecules.

With a strong focus on clinical translation Glu-urea-Lys-HBED-CC-IRDye800CW and Glu-urea-Lys-HBED-CC-DyLight800 were considered for further proof-of-concept studies as they allow fluorescence-guidance in the near infrared part of the light spectrum, which has been proven to be ideal for intraoperative fluorescence detection as near infrared light can still be detected underneath blood and tissue in about 1 cm depth. In addition, this approach is supported by clinically established instruments such as the da Vinci surgical system*(7,8)*. Radio-guidance can optionally be performed with this dual-labeled compound in case of tumor lesions located deeper in the pelvis beyond the fluorescence detection limit as the chelator HBED-CC also allows the labeling with

radionuclides suitable for radio-guidance. Clinical protocols of specific radio-guidance have recently been published providing a proof of concept with this modality*(5)*.

Interestingly, despite comparable high tumor uptake of both conjugates, ^{68}Ga-Glu-urea-Lys-HBED-CC-IRDye800CW shows a higher specificity emphasized by excellent tumor-to-background-ratios at one hour with even increasing values up to six hours post injection. Due the slightly enhanced background activity of ^{68}Ga-Glu-urea-Lys-HBED-CC-DyLight800, which might be attributed to the chemical characteristics of the dye, further *in vivo* proof-of-concept studies were conducted with ^{68}Ga-Glu-urea-Lys-HBED-CC-IRDye800CW. These studies demonstrated the feasibility of ^{68}Ga-Glu-urea-Lys-HBED-CC-IRDye800CW as a small-molecule based dual-modality probe. In small-animal PET studies tumors were clearly visualized with high contrast. A specific fluorescence signal could subsequently be detected in PSMA-expressing tissue providing the surgeon visual information for the exact localization of relevant PSMA-positive malign tissue and its discrimination from healthy surrounding tissue. Compared to the clinically established PET-tracer PSMA-11, the considerably increased tumor uptake with remaining high specificity and successful proof-of-concept studies are encouraging us to focus on future clinical translation.

CONCLUSION

PSMA-targeting dual-modality probes have the potential to considerably improve the outcome of prostate cancer therapy providing the surgeon precious information by combined radioactive and fluorescence signal. The PSMA-11 based dual-labeled compound ^{68}Ga-Glu-urea-Lys-HBED-CC-IRDye800CW is characterized by high and fast PSMA-specific tumor enrichment with rapid background clearance. This approach

allows precise pre-, intra- and optional postoperative detection of tumor lesions. These features are very promising for establishing a dual-labeled modality supported treatment regimen for prostate cancer.

DISCLOSURE

This study was supported by the VIP+ grant VP00130, Federal Ministry of Education & Research (BMBF), Germany. Technical support was kindly provided by KARL STORZ and Intuitive Surgical**.**

ACKNOWLEDGEMENTS

Biodistribution and small-animal PET studies were kindly performed by Karin Leotta and Ursula Schierbaum (both German Cancer Research Center, Heidelberg, Germany). Confocal Microscopy was kindly supported by the Core Facility Light Microscopy (German Cancer Research Center, Heidelberg, Germany). We gratefully thank PD Dr. med. Arianeb Mehrabi (University Hospital Heidelberg, Heidelberg, Germany) and his team for supporting the animal studies.

REFERENCES

1. Perera M, Papa N, Christidis D, et al. Sensitivity, specificity, and predictors of positive 68Ga-prostate-specific membrane antigen positron emission tomography in advanced prostate cancer: a systematic review and meta-analysis. *Eur Urol.* 2016;70:926-937.
2. Weckermann D, Dorn R, Trefz M, Wagner T, Wawroschek F, Harzmann R. Sentinel lymph node dissection for prostate cancer: experience with more than 1,000 patients. *J Urol.* 2007;177:916-920.
3. Mattei A, Fuechsel FG, Bhatta Dhar N, et al. The template of the primary lymphatic landing sites of the prostate should be revisited: results of a multimodality mapping study. *Eur Urol.* 2008;53:118-125.
4. Stephenson AJ, Eggener SE, Hernandez AV, et al. Do margins matter? The influence of positive surgical margins on prostate cancer-specific mortality. *Eur Urol.* 2014;65:675-680.
5. Maurer T, Weirich G, Schottelius M, et al. Prostate-specific membrane antigen-radioguided surgery for metastatic lymph nodes in prostate cancer. *Eur Urol.* 2015;68:530-534.
6. van den Berg NS, Buckle T, KleinJan GH, van der Poel HG, van Leeuwen FWB. Multispectral fluorescence imaging during robot-assisted laparoscopic sentinel node biopsy: a first step towards a fluorescence-based anatomic roadmap. *Eur Urol.* 2017;72:110-117.
7. Brouwer OR, van den Berg NS, Matheron HM, et al. A hybrid radioactive and fluorescent tracer for sentinel node biopsy in penile carcinoma as a potential replacement for blue dye. *Eur Urol.* 2014;65:600-609.
8. van der Poel HG, Buckle T, Brouwer OR, Valdes Olmos RA, van Leeuwen FW. Intraoperative laparoscopic fluorescence guidance to the sentinel lymph node in prostate cancer patients: clinical proof of concept of an integrated functional imaging approach using a multimodal tracer. *Eur Urol.* 2011;60:826-833.
9. Schulke N, Varlamova OA, Donovan GP, et al. The homodimer of prostate-specific membrane antigen is a functional target for cancer therapy. *Proc Natl Acad Sci U S A.* 2003;100:12590-12595.
10. Wright GL, Jr., Haley C, Beckett ML, Schellhammer PF. Expression of prostate-specific membrane antigen in normal, benign, and malignant prostate tissues. *Urol Oncol.* 1995;1:18-28.
11. Hillier SM, Kern AM, Maresca KP, et al. 123I-MIP-1072, a small-molecule inhibitor of prostate-specific membrane antigen, is effective at monitoring tumor response to taxane therapy. *J Nucl Med.* 2011;52:1087-1093.
12. Eder M, Schafer M, Bauder-Wust U, et al. (68)Ga-Complex lipophilicity and the targeting property of a urea-based PSMA inhibitor for PET imaging. *Bioconjug Chem.* 2012;23:688-697.
13. Benesova M, Schafer M, Bauder-Wust U, et al. Preclinical evaluation of a tailor-made DOTA-conjugated PSMA inhibitor with optimized linker moiety for imaging and endoradiotherapy of prostate cancer. *J Nucl Med.* 2015;56:914-920.
14. Weineisen M, Simecek J, Schottelius M, Schwaiger M, Wester H-J. Synthesis and preclinical evaluation of DOTAGA-conjugated PSMA ligands for functional imaging and endoradiotherapy of prostate cancer. *EJNMMI Res.* 2014;4:63.
15. Foss CA, Mease RC, Fan H, et al. Radiolabeled small-molecule ligands for prostate-specific membrane antigen: in vivo imaging in experimental models of prostate cancer. *Clin Cancer Res.* 2005;11:4022-4028.
16. Smith-Jones PM, Vallabahajosula S, Goldsmith SJ, et al. In vitro characterization of radiolabeled monoclonal antibodies specific for the extracellular domain of prostate-specific membrane antigen. *Cancer Res.* 2000;60:5237-5243.
17. Chen Y, Dhara S, Banerjee SR, et al. A low molecular weight PSMA-based fluorescent imaging agent for cancer. *Biochem Biophys Res Commun.* 2009;390:624-629.

18. Liu T, Wu LY, Hopkins MR, Choi JK, Berkman CE. A targeted low molecular weight near-infrared fluorescent probe for prostate cancer. *Bioorg Med Chem Lett.* 2010;20:7124-7126.

19. Nakajima T, Mitsunaga M, Bander NH, Heston WD, Choyke PL, Kobayashi H. Targeted, activatable, in vivo fluorescence imaging of prostate-specific membrane antigen (PSMA) positive tumors using the quenched humanized J591 antibody-indocyanine green (ICG) conjugate. *Bioconjug Chem.* 2011;22:1700-1705.

20. Humblet V, Lapidus R, Williams LR, et al. High-affinity near-infrared fluorescent small-molecule contrast agents for in vivo imaging of prostate-specific membrane antigen. *Mol Imaging.* 2005;4:448-462.

21. Lutje S, Rijpkema M, Franssen GM, et al. Dual-modality image-guided surgery of prostate cancer with a radiolabeled fluorescent anti-PSMA monoclonal antibody. *J Nucl Med.* 2014;55:995-1001.

22. Banerjee SR, Pullambhatla M, Byun Y, et al. Sequential SPECT and optical imaging of experimental models of prostate cancer with a dual modality inhibitor of the prostate-specific membrane antigen. *Angew Chem Int Ed Engl.* 2011;50:9167-9170.

23. Afshar-Oromieh A, Haberkorn U, Eder M, Eisenhut M, Zechmann CM. [68Ga]Gallium-labelled PSMA ligand as superior PET tracer for the diagnosis of prostate cancer: comparison with 18F-FECH. *Eur J Nucl Med Mol Imaging.* 2012;39:1085-1086.

24. Afshar-Oromieh A, Malcher A, Eder M, et al. PET imaging with a [(68)Ga]gallium-labelled PSMA ligand for the diagnosis of prostate cancer: biodistribution in humans and first evaluation of tumour lesions. *Eur J Nucl Med Mol Imaging.* 2013;40:486-495.

25. Schafer M, Bauder-Wust U, Leotta K, et al. A dimerized urea-based inhibitor of the prostate-specific membrane antigen for 68Ga-PET imaging of prostate cancer. *EJNMMI Res.* 2012;2:23.

26. Schuhmacher J, Maier-Borst W. A new Ge-68/Ga-68 radioisotope generator system for production of Ga-68 in dilute HCl. *Int J Appl Radiat Isot.* 1981;32:31–36.

27. Baranski AC, Schafer M, Bauder-Wust U, et al. Improving the imaging contrast of 68Ga-PSMA-11 by targeted linker design: charged spacer moieties enhance the pharmacokinetic properties. *Bioconjug Chem.* 2017;28:2485-2492.

28. Hope TA, Aggarwal R, Chee B, et al. Impact of Ga-68 PSMA-11 PET on management in patients with biochemically recurrent prostate cancer. *J Nucl Med.* 2017.

29. Zhang AX, Murelli RP, Barinka C, et al. A remote arene-binding site on prostate specific membrane antigen revealed by antibody-recruiting small molecules. *J Am Chem Soc.* 2010;132:12711-12716.

30. Maung J, Mallari JP, Girtsman TA, et al. Probing for a hydrophobic a binding register in prostate-specific membrane antigen with phenylalkylphosphonamidates. *Bioorg Med Chem.* 2004;12:4969-4979.

Figures and Tables

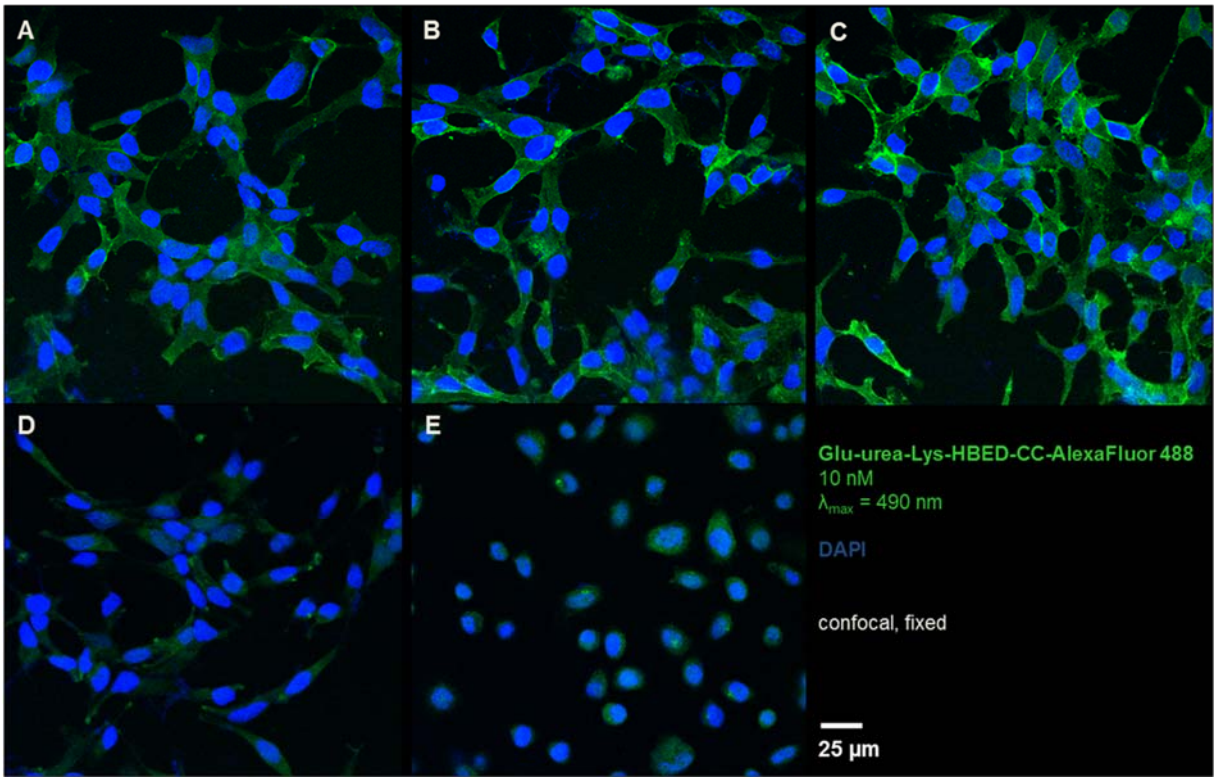

Figure 1 *Specific cell binding and internalization in confocal microscopy. LNCaP cells were incubated with 10 nM non-complexed Glu-urea-Lys-HBED-CC-AlexaFluor488 for 5 (A), 15 (B), 30 (C) min at room temperature, respectively, and fixed with paraformaldehyde. For blocking studies 2-PMPA was added and simultaneously incubated for 30 min (D). PC3 cells as a negative control were incubated with 10 nM non-complexed ligand for 30 min at RT (E).*

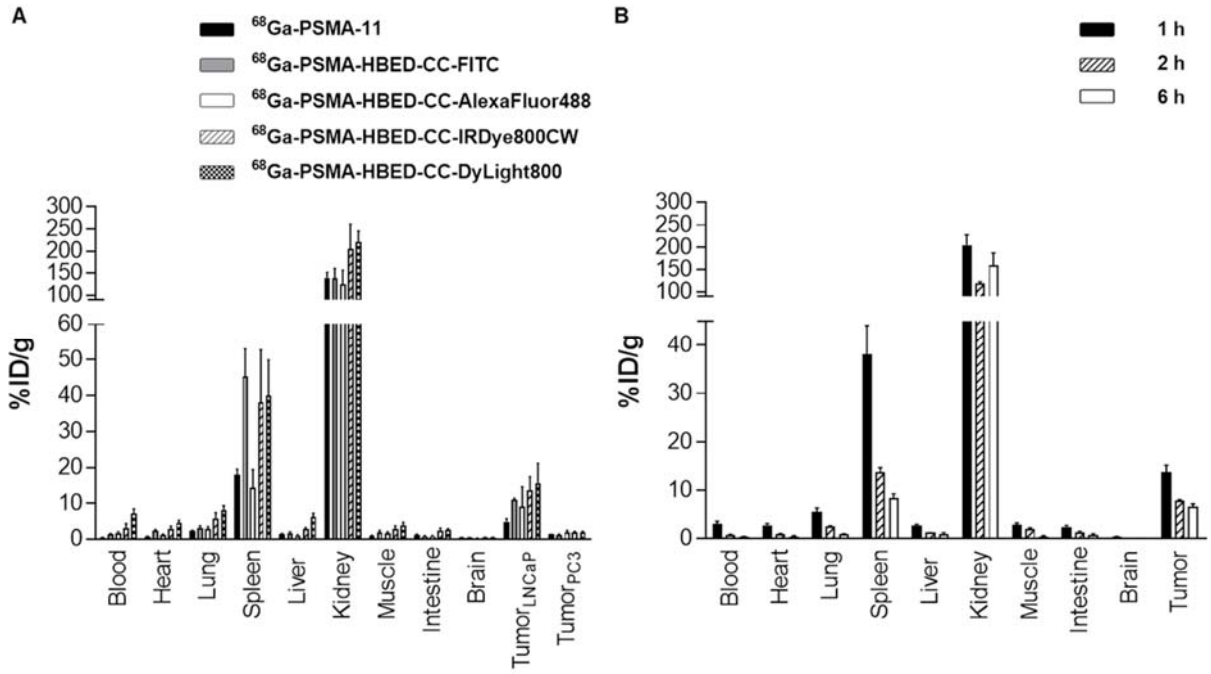

Figure 2 *Organ distribution of 60 pmol of ^{68}Ga labeled Glu-urea-Lys-HBED-CC-Dye conjugates at one hour post injection in comparison to the reference ^{68}Ga-PSMA-11 (27)(A) and 60 pmol of ^{68}Ga-Glu-urea-Lys-HBED-CC-IRDye800CW at one, two and six hours post injection (B). Data are expressed as mean % ID/g tissue ± SD (n=3).*

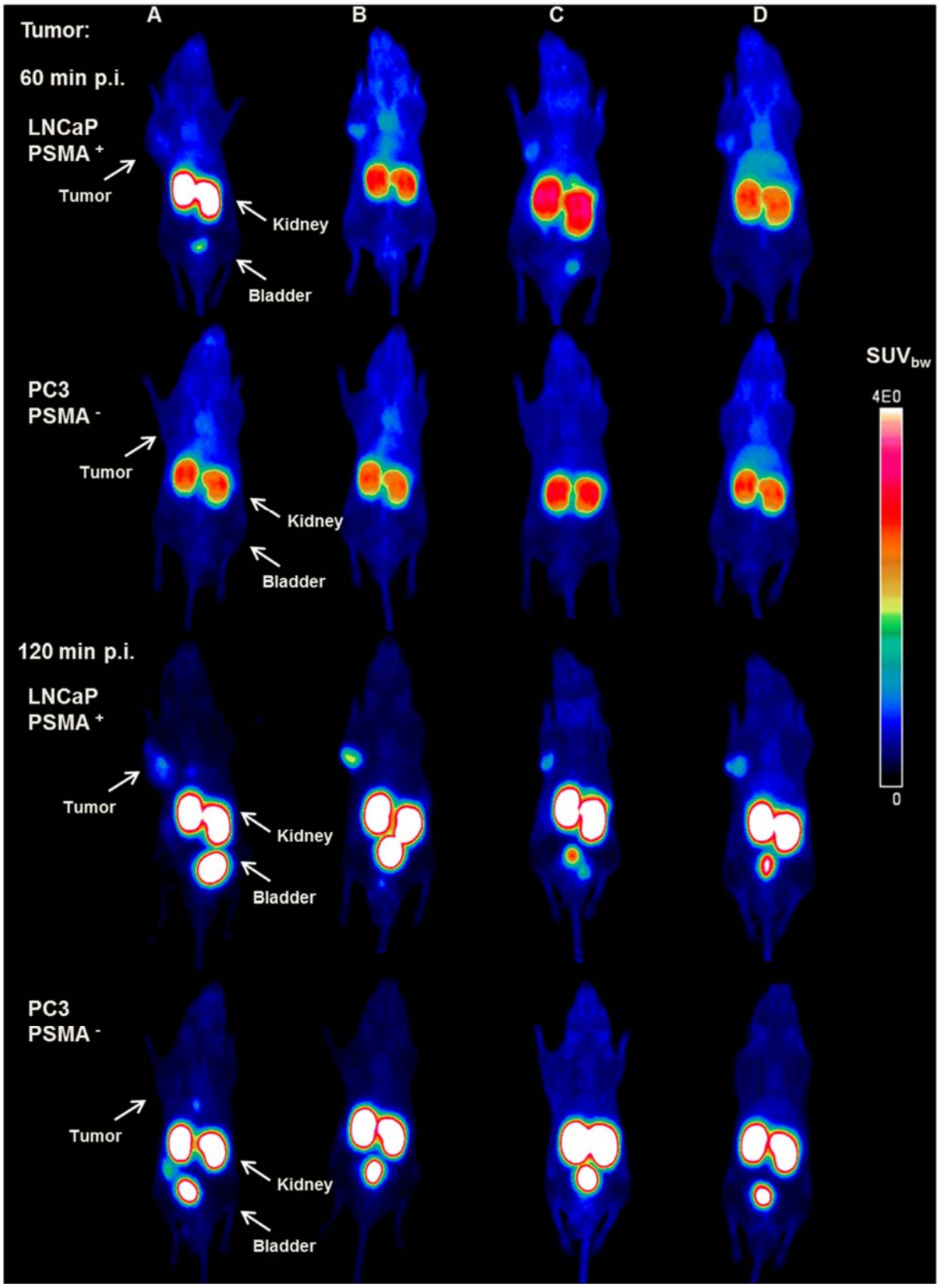
A
B
C
D
Tumor:
60 min p.i.
LNCaP
PSMA +
Tumor
Kidney
Bladder
PC3
PSMA -
Tumor
Kidney
Bladder
120 min p.i.
LNCaP
PSMA +
Tumor
Kidney
Bladder
PC3
PSMA -
Tumor
Kidney
Bladder
SUVbw
4E0
0

447

448 **Figure 3** *Maximum intensity projections derived from μPET imaging of LNCaP- (upper*
449 *rows) or PC3- (lower rows) tumor-bearing athymic nude mice (right trunk). Scans were*
450 *evaluated 60 and 120 min post-injection of 0.5 nmol of ^{68}Ga-labeled (~50 MBq) Glu-*
451 *urea-Lys-HBED-CC-FITC (A), Glu-urea-Lys-HBED-CC-AlexaFluor488 (B), Glu-urea-*
452 *Lys-HBED-CC-IRDye800CW (C) and Glu-urea-Lys-HBED-CC-DyLight800 (D).*
453 *SUV=standardized uptake value.*

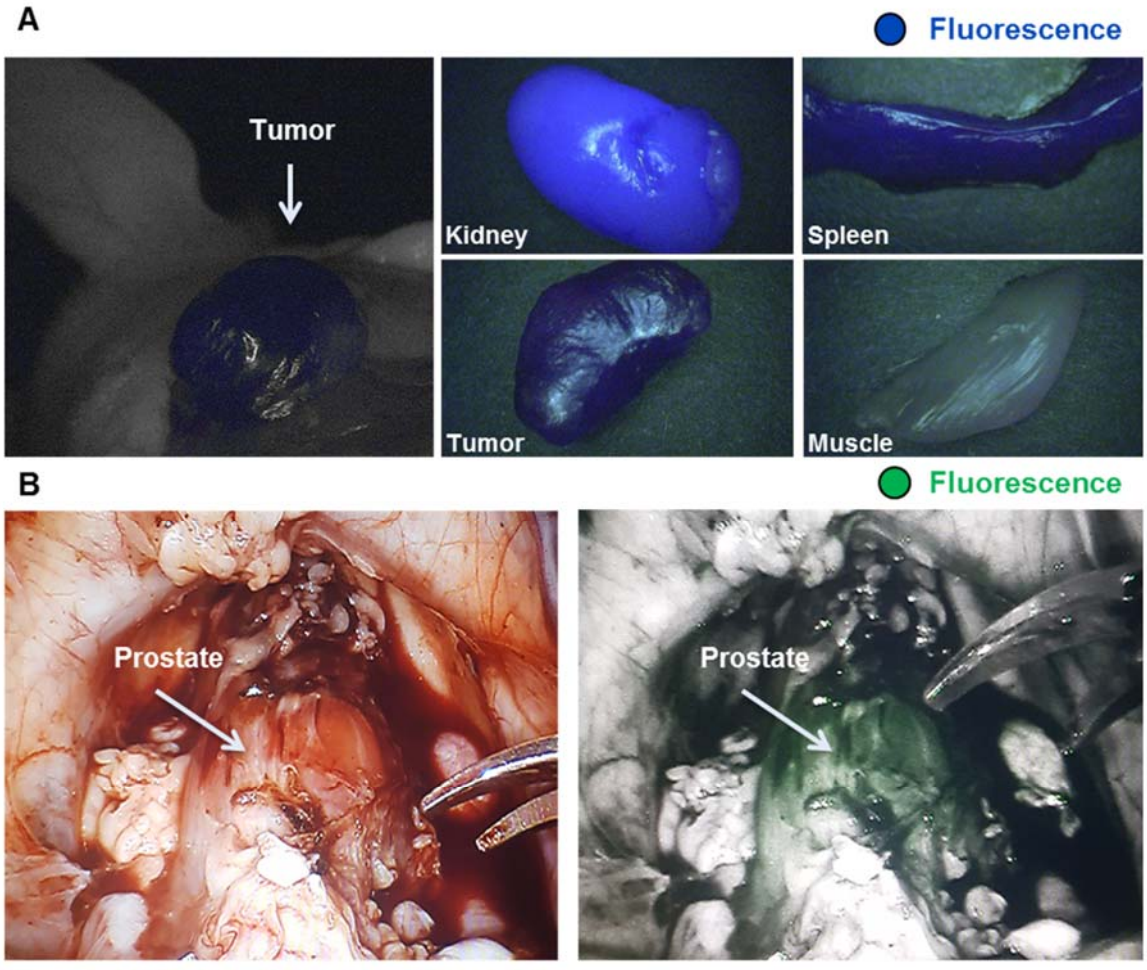

454

455 **Figure 4** *Proof-of-concept fluorescence-guided surgery studies in tumor-bearing mice*
456 *(A) and healthy pigs (B). 0.5 nmol ^{68}Ga-Glu-urea-Lys-HBED-CC-IRDye800CW were*

injected in mice (LNCaP tumor xenograft) for μPET imaging, followed by fluorescence detection after 120 min ex vivo (IMAGE1 S system, fluorescence signal: blue). After pre-imaging acquisition of background fluorescence with da Vinci FireFly System Glu-urea-Lys-HBED-CC-IRDye800CW (30 μg/kg) were intravenously injected. Fluorescence-guided prostatectomy accompanied by in vivo and ex vivo fluorescence detection was performed one hour post injection (fluorescence signal: green).

464 **Table 1** *Analytic data of the compounds.*

Compound	m/z (g/mol, M_{calc})	m/z* (M_{found})	Chemical yield [%]†
Glu-urea-Lys-HBED-CC-FITC	1355.4	1356.9	23
Glu-urea-Lys-HBED-CC-AlexaFluor488	1478.4	1481.5	27
Glu-urea-Lys-HBED-CC-IRDye800CW	1950.2	1951.4	35
Glu-urea-Lys-HBED-CC-DyLight800	1902.1	1901.9	18

465 * Mass spectrometry of non-labeled ligand, † Chemical yields refer to the fluorescent dye conjugation
466 reaction to Glu-urea-Lys[Fe(HBED-CC)]-PEG_2-NH_2

467

Table 2 *Cell binding and internalization of the dye-conjugates in comparison to PSMA-11 (25,27)*.*

Compound	Specifically cell surface bound [%IA/10^5 cells]†	Specifically internalized [%IA/10^5 cells]†	IC_{50} [nM]‡	IC_{50} [nM]§
PSMA-11	18.31 ± 0.71	3.54 ± 0.28	19.19 ± 7.42	12.1 ± 2.1
Glu-urea-Lys-HBED-CC-FITC	1.28 ± 0.20	4.89 ± 0.93	11.14 ± 1.16	10.52 ± 1.47
Glu-urea-Lys-HBED-CC-AlexaFluor488	5.22 ± 0.25	14.96 ± 0.81	13.32 ± 0.83	25.59 ± 3.93
Glu-urea-Lys-HBED-CC-IRDye800CW	13.62 ± 4.79	18.70 ± 7.03	24.54 ± 5.70	35.54 ± 2.94
Glu-urea-Lys-HBED-CC-DyLight800	10.50 ± 3.64	13.88 ± 7.04	21.41 ± 1.90	21.23 ± 4.26

***** Data are expressed as mean ± SD (n=3)

† ^{68}Ga-labeled compounds. Specific cell uptake was determined by blockage using 500 µM 2-PMPA. Values are expressed as % of applied radioactivity (IA) bound to 10^5 cells.

‡ metal-free ligands

§ $^{69/71}$Ga-labeled compounds

Online Supplemental Material

Table of Content

Characterization of the precursor Glu-urea-Lys-HBED-CC-PEG$_2$-NH$_2$

Supplemental Figure 1. HPLC run of the precursor Glu-urea-Lys[Fe(HBED-CC)]-PEG$_2$-NH$_2$ with the system Agilent 1100 series (Agilent Technologies, Santa Clara, California, USA) equipped with a Chromolith RP-18e column, 100×4.6 mm (Merck, Darmstadt, Germany). Analyses were performed using a linear gradient (0.1% aqueous TFA (A) to 100% B (0.1% TFA in CH_3CN)) in 5 min at a flow rate of 2 mL/min. The chromatogram was recorded at 214 nm. The compound was formulated in H_2O/ CH_3CN.

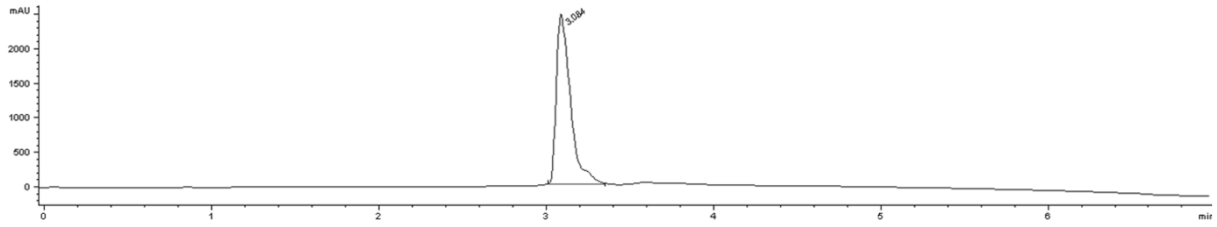

Supplemental Figure 2. High resolution mass of the metal-free compound Glu-urea-Lys-HBED-CC-PEG$_2$-NH$_2$ solved in MeCN/MeOH was performed using Bruker apex-Qe FTICR mass spectrometer.

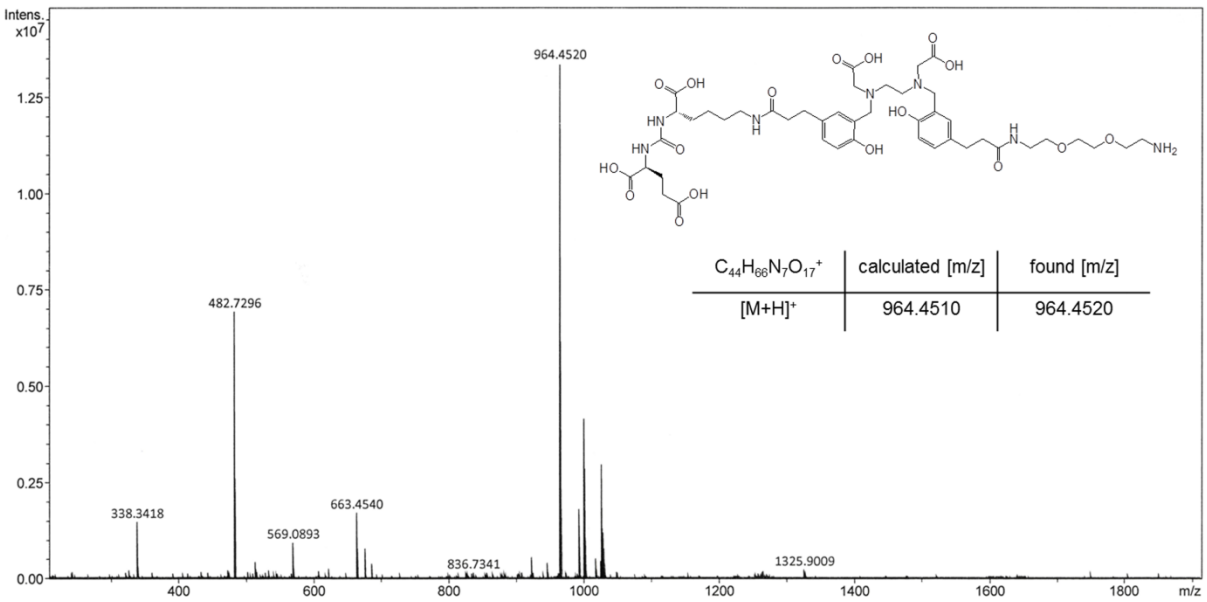

Supplemental Figure 3. ^{1}H NMR spectrum of metal-free Glu-urea-Lys-HBED-CC-PEG$_2$-NH$_2$ (400 MHz, 300 K, DMSO-d6)

δ (ppm) = 8.01 (t, *J* = 5.6 Hz, 1H), 7.86 (t, *J* = 5.3 Hz, 1H), 6.98 – 6.88 (m, 4H), 6.64 (d, *J* = 8.0 Hz, 2H), 6.40 (t, *J* = 7.9 Hz, 2H), 4.09 – 3.97 (m, 2H), 3.69 (d, *J* = 9.1 Hz, 4H), 3.60 (t, *J* = 5.1 Hz, 2H), 3.56 – 3.45 (m, 4H), 3.36 (t, *J* = 5.7 Hz, 2H), 3.23 – 3.08 (m, 6H), 3.04 – 2.92 (m, 4H), 2.70 (d, *J* = 30.5 Hz, 7H), 2.37 – 2.16 (m, 6H), 1.87 (dt, *J* = 13.7, 6.5 Hz, 1H), 1.77 – 1.67 (m, 1H), 1.62 (dd, *J* = 13.4, 5.4 Hz, 1H), 1.49 (dt, *J* = 21.1, 7.3 Hz, 1H), 1.39 – 1.19 (m, 6H).

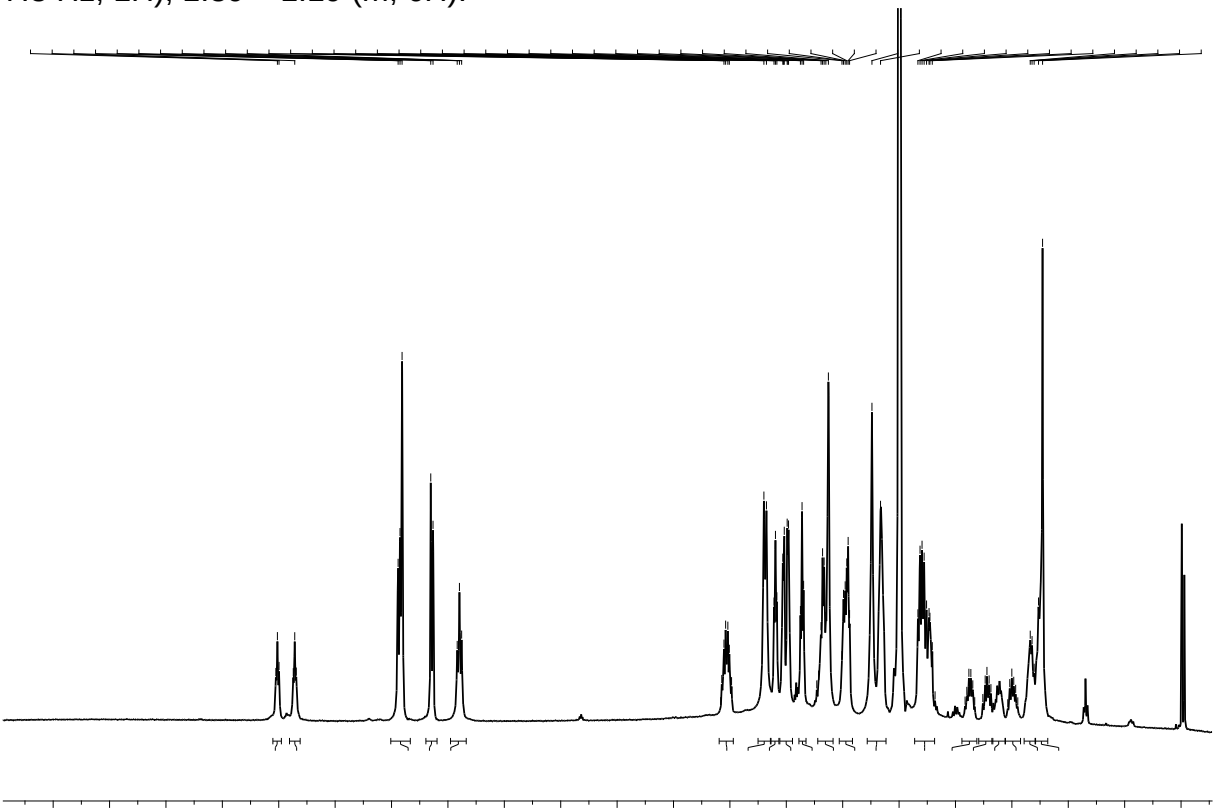

Supplemental Figure 4. ^{13}C NMR spectrum of metal-free Glu-urea-Lys-HBED-CC-PEG$_2$-NH$_2$ (101 MHz, 300 K, DMSO-d6)

δ (ppm) = 174.7, 174.4, 173.9, 172.4, 172.2, 171.8, 171.4, 157.4, 154.9, 131.2, 131.1, 130.3, 130.6, 128.7, 128.6, 121.8, 115.4, 115.3, 69.5, 69.4, 69.1, 66.7, 55.2, 55.0, 54.1, 54.0, 52.4, 52.0, 49.2, 38.5, 38.2, 37.6, 37.5, 31.8, 30.5, 30.4, 30.2, 29.0, 28.8, 28.7, 27.8, 26.6, 22.6, 14.0.

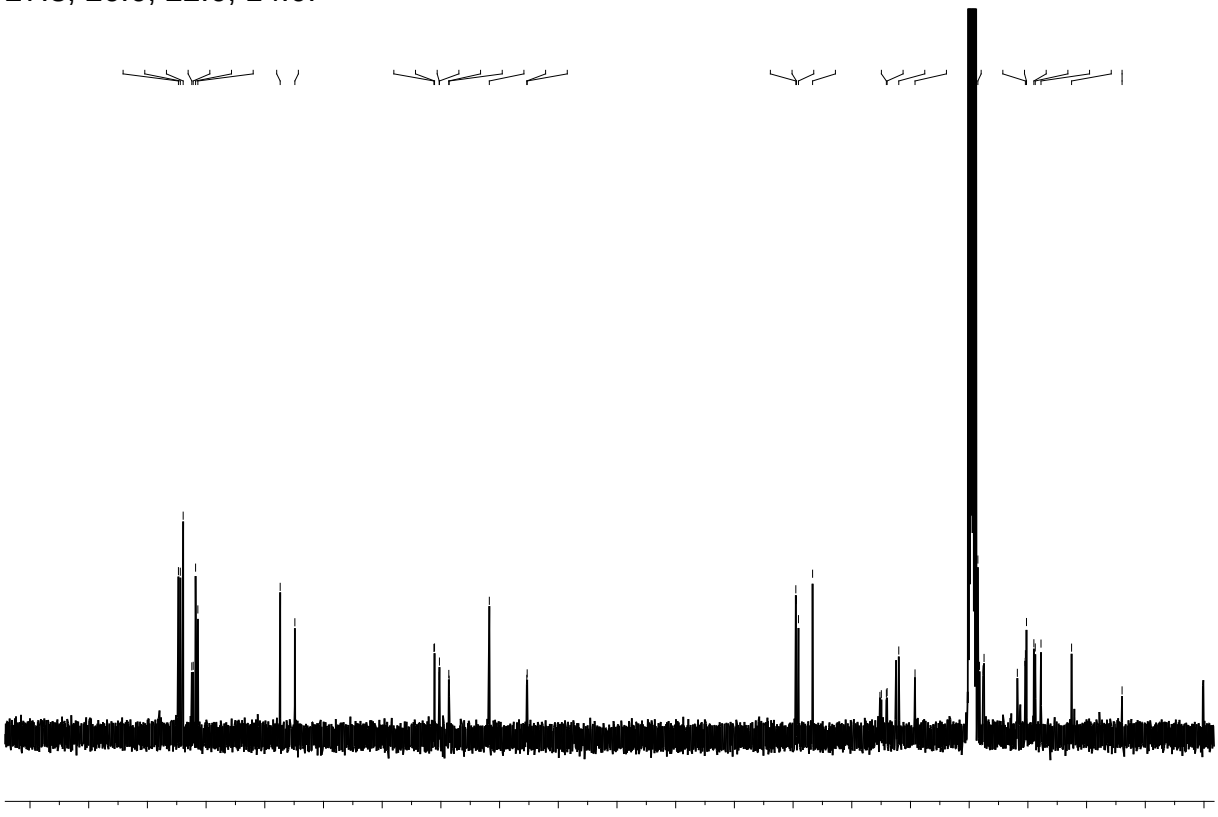

Supplemental Figure 5. ^{13}C NMR DEPT spectrum of metal-free Glu-urea-Lys-HBED-CC-PEG_2-NH_2 (101 MHz, 300 K, DMSO-d6)

δ (ppm) = 130.1 (CH_{arom}), 130.0 (CH_{arom}), 128.4 (CH_{arom}), 128.4 (CH_{arom}), 115.1 (CH_{arom}), 115.1 (CH_{arom}), 69.2 (CH_2), 69.2 (CH_2), 68.8 (CH_2), 66.4 (CH_2), 55.0 (CH_2), 54.7 (CH_{alkyl}), 53.9 (CH_2), 53.7 (CH_2), 52.2 (CH_2), 51.8 (CH_{alkyl}), 49.0 (CH_2), 38.3 (CH_2), 38.0 (CH_2), 37.4 (CH_2), 37.2 (CH_2), 31.6 (CH_2), 30.2 (CH_2), 30.17 (CH_2), 30.0 (CH_2), 28.8 (CH_2), 28.7 (CH_2), 28.5 (CH_2), 27.5 (CH_2), 22.3 (CH_2).

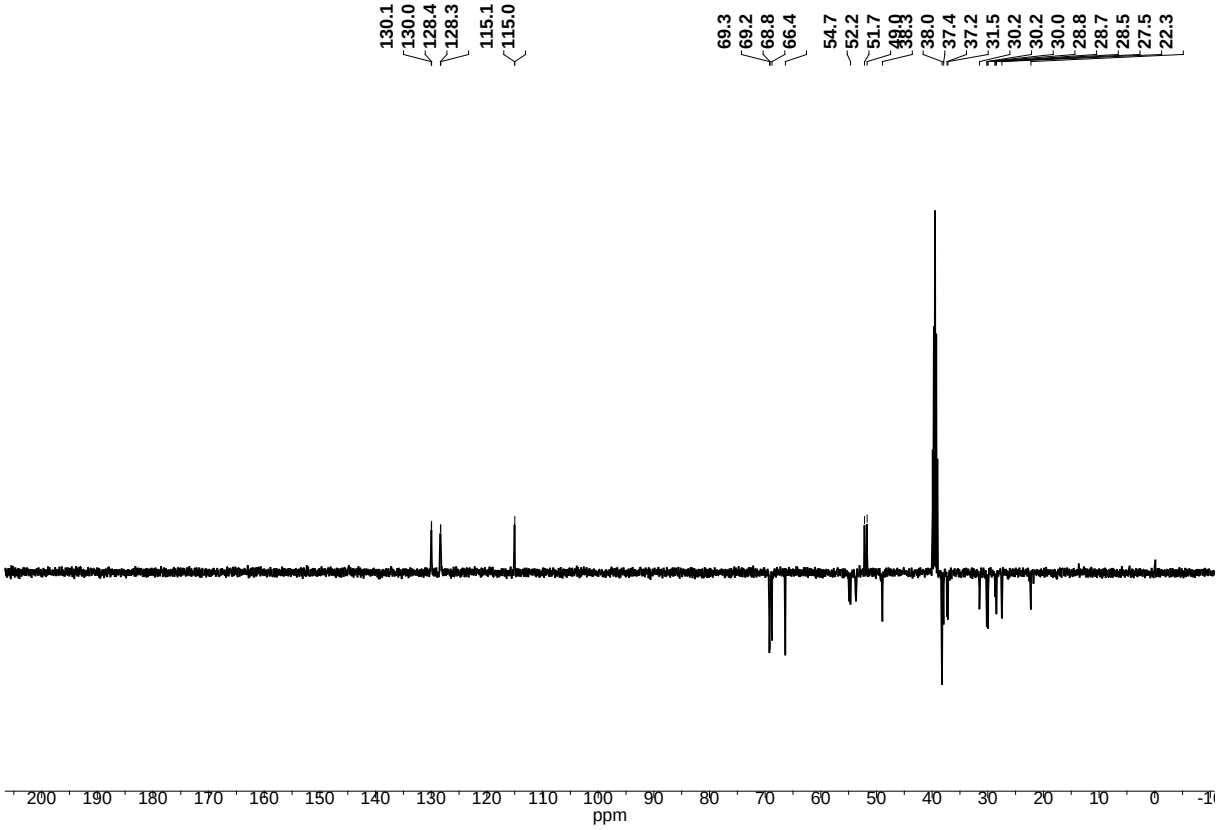

Core Structure of Dual-Labeled PSMA-Inhibitors

Supplemental Figure 6. Core structure of the synthesized dye-conjugates based on PSMA-11.

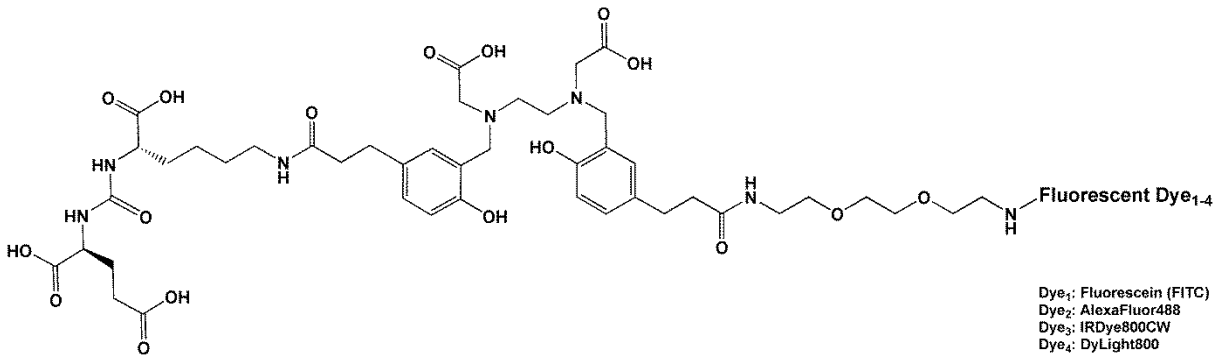

(Radio)chemical characterization of Glu-urea-Lys-HBED-CC-dye conjugates

HPLC methods

Preparative HPLC was performed with LaPrep-System P110 (VWR, Darmstadt, Germany) equipped with a NUCLEODUR® Sphinx RP column and a variable UV detector (P314, VWR, Darmstadt, Germany) with a flow rate of 20 ml/min. The system Agilent 1100 series (Agilent Technologies, Santa Clara, California, USA) was equipped with Chromolith RP-18e (100×10 mm; Merck, Darmstadt, Germany) for semipreparative HPLC and Chromolith RP-18e (100×4.6 mm; Merck, Darmstadt, Germany) for analytical HPLC. UV absorbance was measured at 214 and 254 nm, respectively.

Supplemental Figure 7. HPLC runs and chemical structures of the compounds Glu-urea-Lys-HBED-CC-FITC, -AlexaFluor488, -IRdye800CW and –DyLight800 with the system Agilent 1100 series (Agilent Technologies, Santa Clara, California, USA) equipped with a Chromolith RP-18e column, 100×4.6 mm (Merck, Darmstadt, Germany). Analytic runs were performed using a linear gradient (0.1% aqueous TFA (A) to 100% B (0.1% TFA in CH_3CN)) in 5 min at a flow rate of 2 mL/min. Chromatograms were recorded at 214 nm. Compounds were solved in DMSO/H_2O/ MeCN.

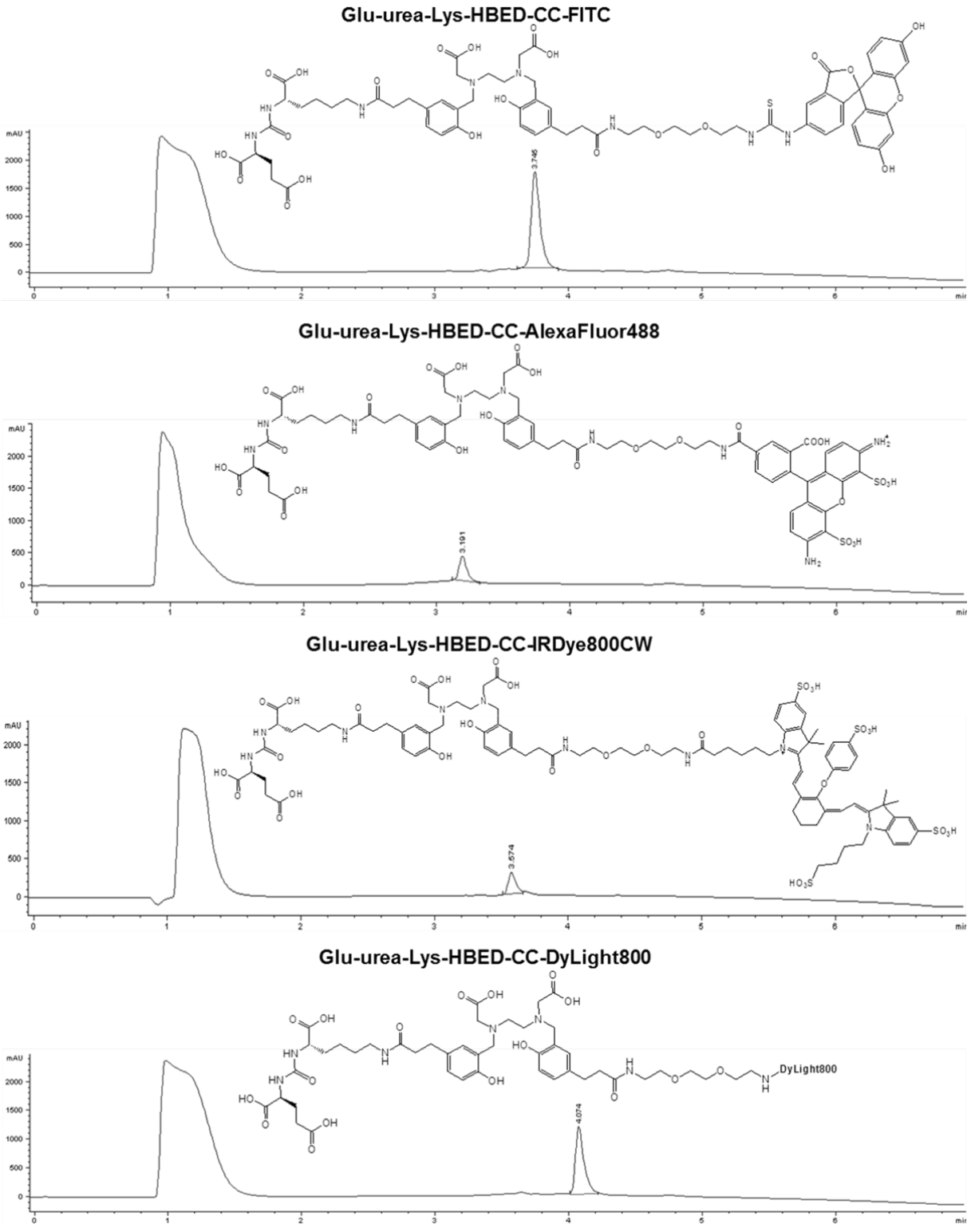

Supplemental Figure 8. Exemplary radio-HPLC of the ^{68}Ga-labeled compound Glu-urea-Lys-HBED-CC-AlexaFluor488 with a Chromolith RP-18e column, 100×4.6 mm (Merck, Darmstadt, Germany). The system L6200 A (Merck-Hitachi, Darmstadt, Germany) was equipped with a gamma detector (Bioscan; Washington, USA). Analyses were performed using a linear gradient (0.1% aqueous TFA (A) to 100% B (0.1% TFA in CH_3CN)) in 5 min at a flow rate of 4 mL/min.

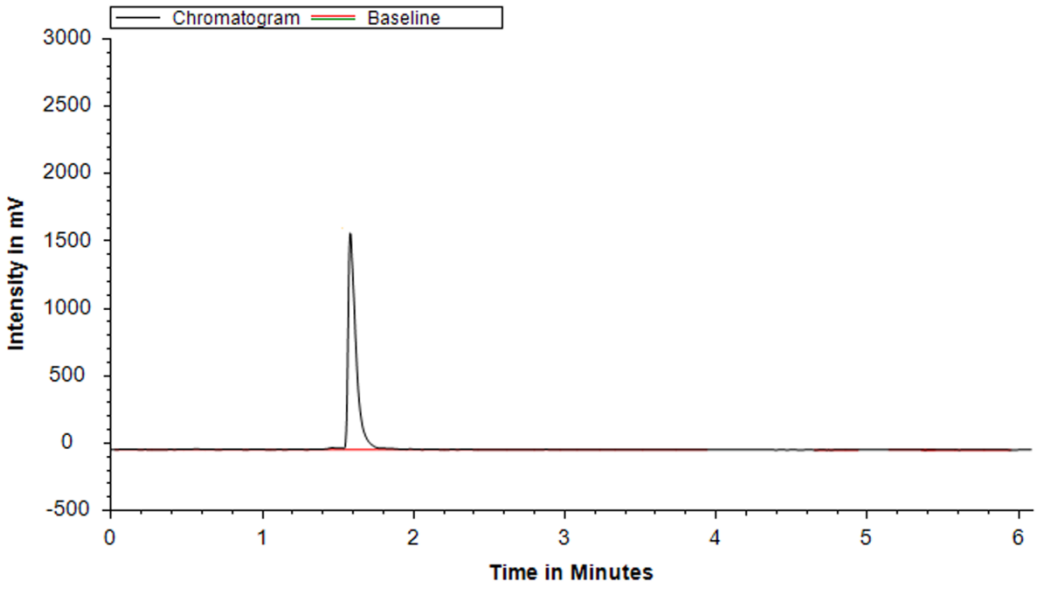

Supplemental Figure 9. Exemplary radio-RP-TLC (60 RP-18F254S; Merck, Darmstadt, Germany) of the ^{68}Ga-labeled compound Glu-urea-Lys-HBED-CC-IRDye800CW (A) and additionally added [^{68}Ga]$GaCl_3$ as a control (B) with 0.1 M sodium citrate as a mobile phase. The RP-TLCs were scanned with miniGITA (Raytest, Straubenhardt, Germany). R_f ([^{68}Ga]$GaCl_3$) = 0.9, R_f ([^{68}Ga]Ga-Peptide) = 0.1).

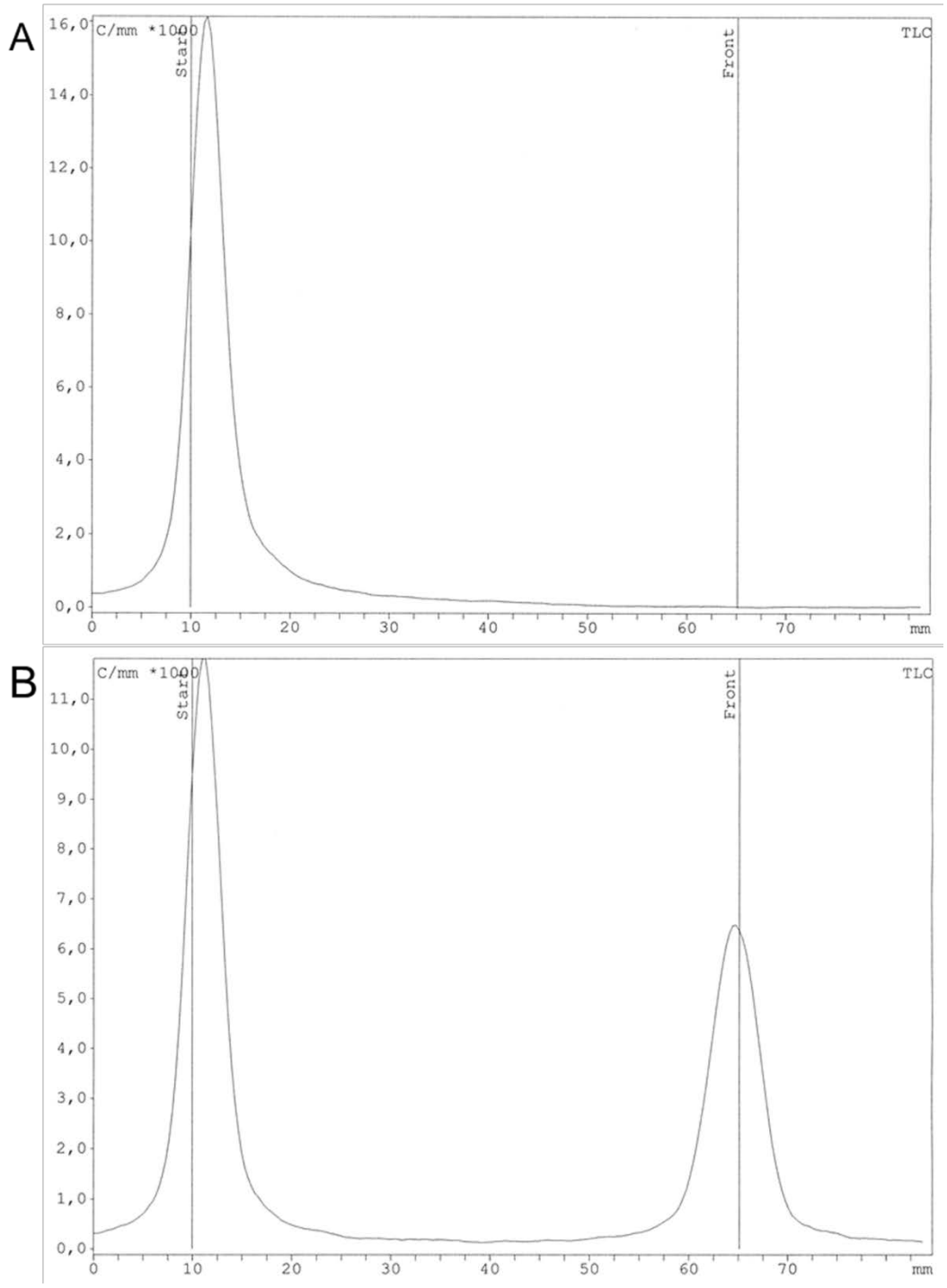

Supplemental Figure 10. Exemplary mass spectrum of the $^{69/71}$Ga-labeled compound Glu-urea-Lys-HBED-CC-IRDye800CW detected with MALDI-MS (Daltonics Microflex, Bruker Daltonics, Bremen, Germany). Gentisinic acid was used as matrix. m/z_{calc} = 2019.7 $[M+H]^+$, m/z_{found} = 2019.4 $[M+H]^+$.

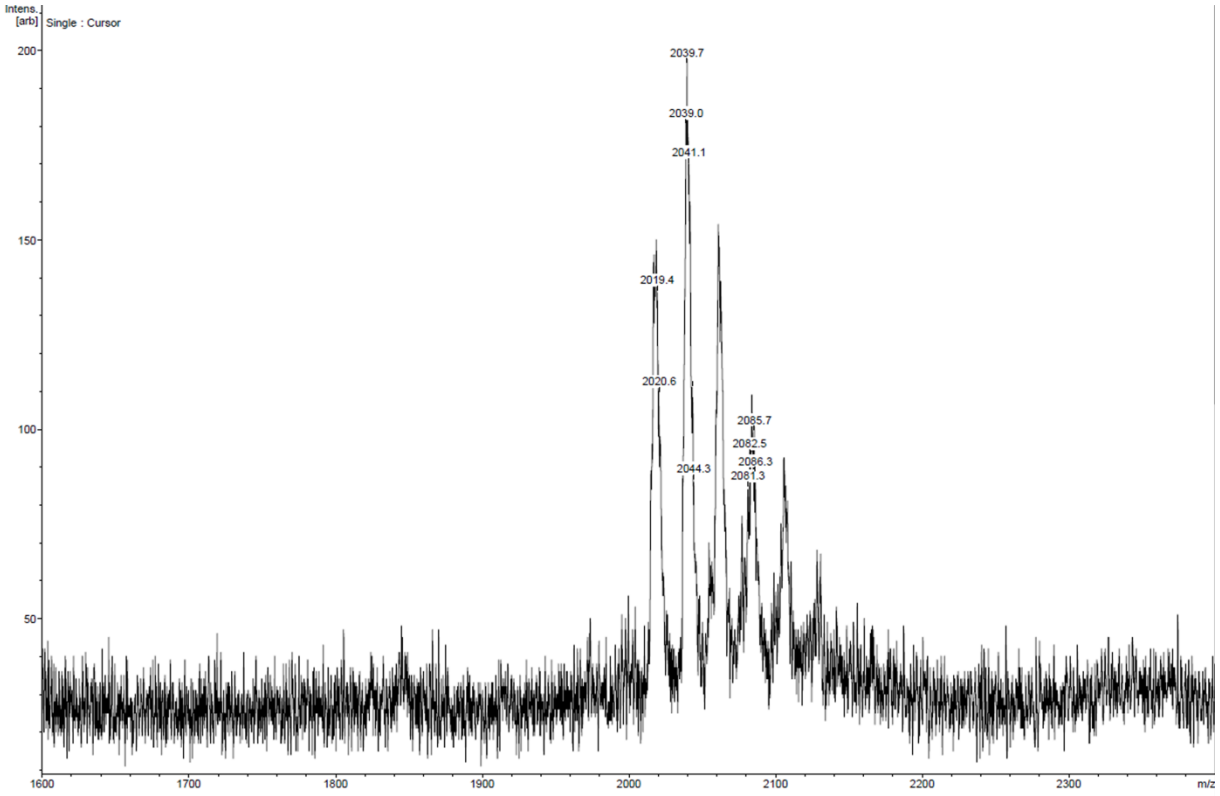

Lipophilicity

Supplemental Table 1. Lipophilicity determined as logD in Octanol/PBS of the ^{68}Ga-labeled compounds in comparison to the reference ^{68}Ga-PSMA-11.

Compound	Lipophilicity determined as logD in Octanol/PBS
^{68}Ga-PSMA-11	- 2.91 ± 0.06
^{68}Ga-Glu-urea-Lys-HBED-CC-FITC	- 2.98 ± 0.09
^{68}Ga-Glu-urea-Lys-HBED-CC-AlexaFluor488	- 2.01 ± 0.39
^{68}Ga-Glu-urea-Lys-HBED-CC-IRDye800CW	- 2.21 ± 0.36
^{68}Ga-Glu-urea-Lys-HBED-CC-DyLight800	- 2.95 ± 0.03

Specific internalization at 4°C

Supplemental Table 2. Specific internalization of the ^{68}Ga-labeled dye-conjugates at 4 °C.

Compound	Specifically cell surface bound [%IA/10^5 cells]†	Specifically internalized [%IA/10^5 cells]†
Glu-urea-Lys-HBED-CC-FITC	0.71 ± 0.06	2.08 ± 0.44
Glu-urea-Lys-HBED-CC-AlexaFluor488	0.51 ± 0.90	9.96 ± 2.67
Glu-urea-Lys-HBED-CC-IRDye800CW	6.36 ± 2.30	6.42 ± 2.27
Glu-urea-Lys-HBED-CC-DyLight800	2.89 ± 2.00	3.97 ± 2.01

† ^{68}Ga-labeled compounds. Specific cell uptake was determined by blockage using 500 µM 2-PMPA. Values are expressed as % of applied radioactivity (IA) bound to 10^5 cells.

Organ Distribution

Supplemental Table 3. Organ distribution of ^{68}Ga-Glu-urea-Lys-HBED-CC-dye conjugates in LNCaP-tumor bearing balb/c nu/nu mice 1 h p.i. in comparison to ^{68}Ga-labeled PSMA-11*†.

	^{68}Ga-PSMA-11	^{68}Ga-Glu-urea-Lys-HBED-CC-FITC	^{68}Ga-Glu-urea-Lys-HBED-CC-AlexaFluor488	^{68}Ga-Glu-urea-Lys-HBED-CC-IRDye800CW	^{68}Ga-Glu-urea-Lys-HBED-CC-DyLight800
Blood	0.53 ± 0.04	1.34 ± 0.40	1.73 ± 0.31	3.04 ±1.36	7.17 ± 1.31
Heart	0.83 ± 0.08	2.22 ± 0.68	1.11 ± 0.28	2.78 ± 0.83	4.55 ± 0.72
Lung	2.36 ± 0.27	3.09 ± 1.07	2.80 ± 0.67	5.60 ± 1.79	8.21 ± 1.16
Spleen	17.88 ± 2.87	45.24 ± 13.48	14.24 ± 5.15	38.12 ± 14.62	39.90 ± 10.06
Liver	1.43 ± 0.19	1.71 ± 0.54	1.02 ± 0.26	2.76 ± 0.51	6.15 ± 1.07
Kidney	139.44 ± 21.40	138.18 ± 39.08	124.75 ± 32.31	204.98 ± 56.24	220.96 ± 24.38
Muscle	1.00 ± 0.24	1.84 ± 1.06	1.67 ± 0.38	2.86 ± 0.88	3.85 ± 0.86
Intestine	1.14 ± 0.46	0.81 ± 0.23	0.81 ± 0.22	2.41 ± 0.72	2.64 ± 0.20
Brain	0.40 ± 0.19	0.31 ± 0.22	0.24 ± 0.03	0.43 ± 0.14	0.51 ± 0.05
Tumor	4.89 ± 1.34	10.86 ± 0.94	9.12 ± 5.47	13.66 ± 3.73	15.62 ± 5.52

***** Data are expressed as mean % ID/g tissue ± SD (n=3)

†Data of ^{68}Ga-labeled PSMA-11 published in Baranski et al. *Bioconjug Chem.* 2017; 28:2485-2492.

Supplemental Table 4. Organ distribution of ^{68}Ga-Glu-urea-Lys-HBED-CC-dye conjugates in PC3- tumor bearing balb/c nu/nu mice 1 h p.i. in comparison to ^{68}Ga-labeled PSMA-11* †.

	^{68}Ga-PSMA-11	^{68}Ga-Glu-urea-Lys-HBED-CC-FITC	^{68}Ga-Glu-urea-Lys-HBED-CC-AlexaFluor488	^{68}Ga-Glu-urea-Lys-HBED-CC-IRDye800CW	^{68}Ga-Glu-urea-Lys-HBED-CC-DyLight800
Blood	0.53 ± 0.04	0.87 ± 0.24	1.54 ± 0.39	1.51 ±0.35	2.29 ± 0.69
Heart	0.83 ± 0.08	1.26 ± 0.15	1.15 ± 0.15	1.22 ± 0.23	1.60 ± 0.32
Lung	2.36 ± 0.27	2.32 ± 0.42	2.74 ± 0.66	3.06 ± 0.63	3.85 ± 1.02
Spleen	17.88 ± 2.87	26.26 ± 3.65	16.77 ± 3.99	19.83 ± 2.50	18.46 ± 1.63
Liver	1.43 ± 0.19	0.99 ± 0.16	0.90 ± 0.11	1.67 ± 0.65	2.62 ± 0.51
Kidney	139.44 ± 21.40	134.15 ± 26.58	123.38 ± 16.42	117.52 ± 20.18	98.88 ± 8.24
Muscle	1.80 ± 0.84	1.22 ± 0.30	1.32 ± 0.38	1.61 ± 0.41	1.30 ± 0.16
Intestine	1.14 ± 0.46	1.36 ± 0.27	1.35 ± 0.58	1.38 ± 0.11	1.30 ± 0.40
Brain	0.40 ± 0.19	0.21 ± 0.02	0.28 ± 0.06	0.21 ± 0.05	0.18 ± 0.01
Tumor	1.30 ± 0.12	1.29 ± 0.18	1.78 ± 0.66	1.85 ± 0.34	1.90 ± 0.32

***** Data are expressed as mean % ID/g tissue ± SD (n=3)

†Data of ^{68}Ga-labeled PSMA-11 published in Schäfer et al. *EJNMMI Res.* 2012;2:23.

Supplemental Table 5. Tumor-to-Organ ratio of ^{68}Ga-Glu-urea-Lys-HBED-CC-dye conjugates in LNCaP-tumor bearing balb/c nu/nu mice 1 h p.i. (n=3) in comparison to ^{68}Ga-labeled PSMA-11 [†].

	^{68}Ga-PSMA-11	^{68}Ga-Glu-urea-Lys-HBED-CC-FITC	^{68}Ga-Glu-urea-Lys-HBED-CC-AlexaFluor488	^{68}Ga-Glu-urea-Lys-HBED-CC-IRDye800CW	^{68}Ga-Glu-urea-Lys-HBED-CC-DyLight800
Blood	9.32	8.10	5.28	4.49	2.18
Heart	5.89	4.89	8.19	4.92	3.43
Lung	2.07	3.51	3.25	2.44	1.90
Spleen	0.27	0.24	0.64	0.36	0.39
Liver	3.42	6.35	8.95	4.94	2.54
Kidney	0.04	0.08	0.07	0.07	0.07
Muscle	4.89	5.90	5.45	4.78	4.06
Intestine	4.29	13.41	11.28	5.66	5.91
Brain	12.23	35.03	38.25	31.39	30.61

[†]Data of ^{68}Ga-labeled PSMA-11 published in Baranski et al. *Bioconjug Chem.* 2017; 28:2485-2492.

Supplemental Table 6. Organ distribution of ^{68}Ga-Glu-urea-Lys-HBED-CC-dye conjugates in LNCaP-tumor bearing balb/c nu/nu mice 1, 2 and 6 h p.i. in comparison to ^{68}Ga-labeled PSMA-11*†.

	^{68}Ga-Glu-urea-Lys-HBED-CC-IRDye800CW	^{68}Ga-PSMA-11	^{68}Ga-Glu-urea-Lys-HBED-CC-IRDye800CW	^{68}Ga-PSMA-11	^{68}Ga-Glu-urea-Lys-HBED-CC-IRDye800CW
	1 h p.i.	1 h p.i.	2 h p.i.	2 h p.i.	6 h p.i.
Blood	3.04 ± 1.36	0.53 ± 0.04	0.76 ± 0.23	0.32 ± 0.14	0.42 ± 0.06
Heart	2.78 ± 0.83	0.83 ± 0.08	1.00 ± 0.11	0.31 ± 0.01	0.51 ± 0.07
Lung	5.60 ± 1.79	2.36 ± 0.27	2.53 ± 0.27	1.19 ± 0.11	0.96 ± 0.07
Spleen	38.12 ± 14.62	17.88 ± 2.87	13.73 ± 1.63	12.41 ± 0.70	8.40 ± 0.85
Liver	2.76 ± 0.51	1.43 ± 0.19	1.21 ± 0.05	0.34 ± 0.05	1.02 ± 0.23
Kidney	204.98 ± 56.24	139.44 ± 21.40	119.56 ± 5.13	129.73 ± 13.77	160.11 ± 27.62
Muscle	2.86 ± 0.88	1.00 ± 0.24	1.96 ± 0.57	2.06 ± 0.36	0.51 ± 0.12
Intestine	2.41 ± 0.72	1.14 ± 0.46	1.37 ± 0.27	1.19 ± 0.35	0.73 ± 0.25
Brain	0.43 ± 0.14	0.40 ± 0.19	0.22 ± 0.01	0.23 ± 0.05	0.09 ± 0.05
Tumor	13.66 ± 3.73	4.89 ± 1.34	7.94 ± 0.19	6.09 ± 0.71	6.57 ± 0.63

***** Data are expressed as mean % ID/g tissue ± SD (n=3)

†Data of ^{68}Ga-labeled PSMA-11 published in Baranski et al. *Bioconjug Chem.* 2017; 28:2485-2492.

Supplemental Table 7. Tumor-to-Organ ratio of ^{68}Ga-Glu-urea-Lys-HBED-CC-IRDye800CW in LNCaP-tumor bearing balb/c nu/nu mice 1,2 and 6 h p.i. (n=3) in comparison to ^{68}Ga-labeled PSMA-11[†].

	^{68}Ga-Glu-urea-Lys-HBED-CC-IRDye800CW	^{68}Ga-PSMA-11	^{68}Ga-Glu-urea-Lys-HBED-CC-IRDye800CW	^{68}Ga-PSMA-11	^{68}Ga-Glu-urea-Lys-HBED-CC-IRDye800CW
	1 h p.i.	1 h p.i.	2 h p.i.	2 h p.i.	6 h p.i.
Blood	4.49	9.32	10.40	18.92	15.56
Heart	4.92	5.89	7.92	19.35	12.87
Lung	2.44	2.07	3.14	5.12	6.88
Spleen	0.36	0.27	0.58	0.49	0.78
Liver	4.94	3.42	6.55	17.99	6.43
Kidney	0.07	0.04	0.07	0.05	0.04
Muscle	4.78	4.89	4.04	2.96	12.85
Intestine	5.66	4.29	5.81	5.11	9.02
Brain	31.39	12.23	36.67	26.71	70.98

[†]Data of ^{68}Ga-labeled PSMA-11 published in Baranski et al. *Bioconjug Chem.* 2017; 28:2485-2492.

Time activity curves

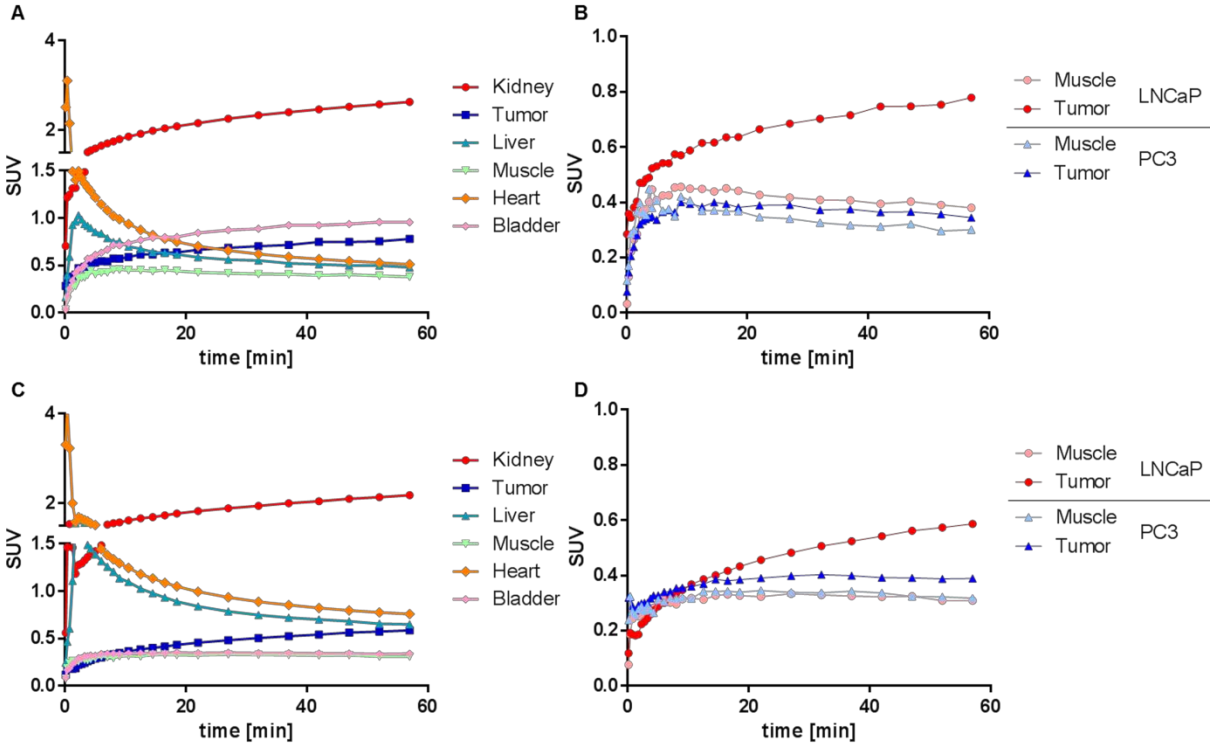

Supplemental Figure 11. µPET imaging derived time activity curves of the ^{68}Ga-labeled compounds Glu-urea-Lys-HBED-CC-IRDye800CW (A,B) and -DyLight800 (C,D) up to 1 h p.i. in LNCaP- and PC3-tumor bearing balb/c nu/nu mice. A and C show the time activity curves related to the most important background organs. B and D highlight the contrast and specificity of the compounds for PSMA-positive tumor tissue (LNCaP xenograft) in comparison to muscle and PSMA-negative tumor tissue (PC3 xenograft).

Proof-of-Concept Fluorescence-Guided Surgery

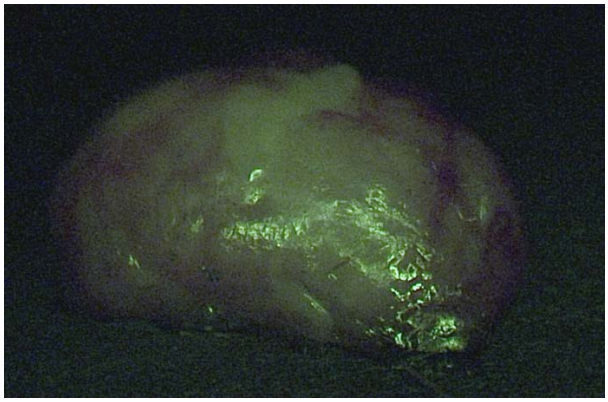

Supplemental Figure 12. Tumor of a LNCaP-tumor bearing balb/c nu/nu mouse as a negative control for the fluorescence signal without any previous treatment or injection. Fluorescence detection was performed *ex vivo* using the IMAGE1 S system (fluorescence signal: blue).

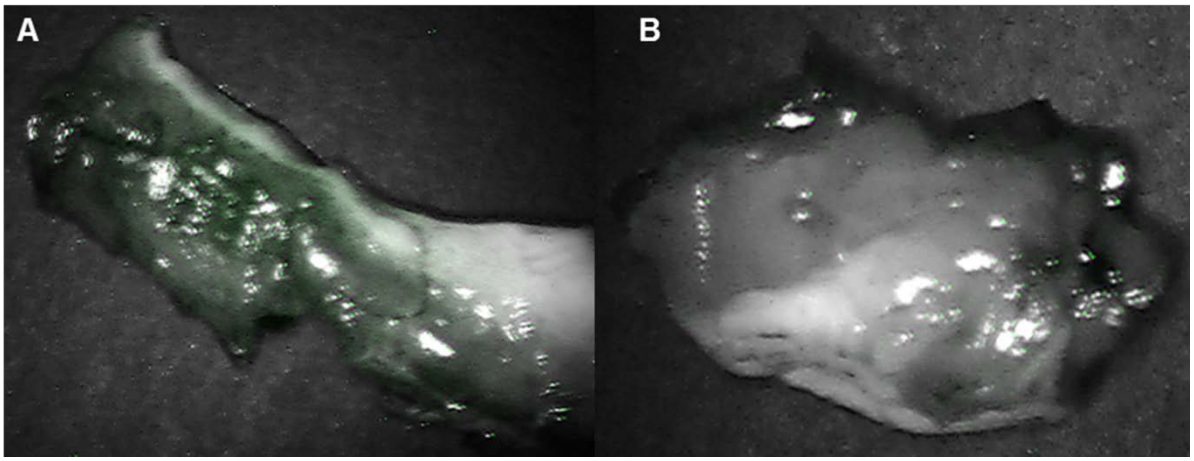

Supplemental Figure 13. Proof-of-concept fluorescence-guided surgery studies in healthy pigs. 1 mg metal-free Glu-urea-Lys-HBED-CC-IRDye800CW (30 µg/kg) were intravenously injected. After *in vivo* fluorescence-guided prostatectomy *ex vivo* fluorescence detection of the prostate (A) and surrounding soft tissue (B) was performed one hour post injection (imaging acquisition with da Vinci FireFly System; fluorescence signal: green).